The Astronomical Journal, 126:1499–1514, 2003 September

CATACLYSMIC VARIABLES FROM THE SLOAN DIGITAL SKY SURVEY. II. THE SECOND YEAR[1]

Paula Szkody,[2] Oliver Fraser,[2] Nicole Silvestri,[2] Arne Henden,[3,4] Scott F. Anderson,[2] James Frith,[2]
Brandon Lawton,[2] Ethan Owens,[2] Sean Raymond,[2] Gary Schmidt,[5] Michael Wolfe,[2]
John Bochanski,[2] Kevin Covey,[2] Hugh Harris,[3] Suzanne Hawley,[2] Gillian R. Knapp,[6]
Bruce Margon,[7] Wolfgang Voges,[8] Lucianne Walkowicz,[2]
J. Brinkmann,[9] and D. Q. Lamb[10]

Received 2003 April 1; accepted 2003 June 5

ABSTRACT

The first full year of operation following the commissioning year of the Sloan Digital Sky Survey (SDSS) has revealed a wide variety of newly discovered cataclysmic variables (CVs). We show the SDSS spectra of 42 CVs observed in 2002, of which 35 are new classifications, four are known dwarf novae (CT Hya, RZ Leo, T Leo, and BZ UMa), one is a known CV identified from a previous quasar survey (Aqr1), and two are known *ROSAT* or FIRST discovered CVs (RX J09445+0357, FIRST J102347.6+003841). The SDSS positions, colors, and spectra of all 42 systems are presented. In addition, the results of follow-up studies of several of these objects identify the orbital periods, velocity curves, and polarization that provide the system geometry and accretion properties. While most of the SDSS discovered systems are faint (greater than 18th magnitude) with low accretion rates (as implied from their spectral characteristics), there are also a few bright objects that may have escaped previous surveys due to changes in the mass transfer rate.

Key words: novae, cataclysmic variables — techniques: photometric — techniques: spectroscopic

1. INTRODUCTION

The commissioning year of the Sloan Digital Sky Survey (SDSS; York et al. 2000), which was released as the Early Data Release (Stoughton et al. 2002), showed the potential for scientific discoveries across a variety of disciplines. For the field of cataclysmic variables (CVs), SDSS is able to find many new CVs, especially those with faint magnitudes that were missed in previous surveys with brighter limits (Szkody et al. 2002, hereafter Paper I). This provides a more accurate picture of the true population of CVs, without the bias of a sample based on high accretion luminosity, and enables the study of the systems that have evolved to the shortest orbital periods and thereby have the lowest mass transfer rates (Howell, Rappaport, & Politano 1997). The SDSS photometry provides accurate magnitudes, colors, and positions, and the spectroscopy usually allows unambiguous identification from the strong hydrogen Balmer and helium emission lines that are the typical signatures of mass transfer in a close binary. Paper I reported 19 new discoveries from the spectra obtained through 2000 December 31, including high-inclination systems, novalikes, and those suspected of harboring magnetic white dwarfs (see Warner 1995 for a complete description of all types of CVs). This paper provides information on an additional 42 CVs found from SDSS spectra obtained through 2001 December 31. Of these 42, seven are previously known CVs from prior X-ray, optical, and radio surveys, three were previously known objects but not classified as CVs, and 32 are new discoveries. Follow-up observations on a number of these systems include photometric light curves, time-resolved spectroscopy, and polarimetry. The resulting analysis allows us to provide a determination of the orbital period, inclination, and magnetic field for several of the CVs.

2. OBSERVATIONS AND REDUCTIONS

The SDSS imaging and spectroscopic instrumentation and reductions are explained in detail in Paper I and in the papers by Fukugita et al. (1996), Gunn et al. (1998), Lupton, Gunn, & Szalay (1999), Hogg et al. (2001), Lupton et al. (2001), Smith et al. (2002), and Pier et al. (2003). As a brief summary, SDSS photometry in five filters (u, g, r, i, and z) is used to select objects by color for later spectroscopy in the range of 3900–6200 Å (blue beam) and 5800–9200 Å (red beam) at a resolving power of ~1800. The spectra are wavelength- and flux-calibrated and corrected for absorption bands, then classified as stars, galaxies, and quasars. The resulting spectra can then be searched by category, redshift, or spectral characteristics.

As explained in Paper I, the selection criteria by color ($u-g < 0.45$, $g-r < 0.7$, $r-i > 0.30$, and $i-z > 0.4$) for the CV category primarily provide spectra of WD plus M binaries, some of which are low mass transfer CVs in which the underlying stars dominate the light. In addition, the color selection for quasars and very blue objects provide spectra of the blue CVs that are disk or white dwarf dominated. A manual search of all the spectra for emission-line

[1] Based on observations obtained with the Sloan Digital Sky Survey and with the Apache Point Observatory 3.5 m telescope, which are owned and operated by the Astrophysical Research Consortium (ARC).

[2] Department of Astronomy, University of Washington, Box 351580, Seattle, WA 98195.
[3] US Naval Observatory, Flagstaff Station, P. O. Box 1149, Flagstaff, AZ 86002-1149.
[4] Universities Space Research Association.
[5] Steward Observatory, University of Arizona, 933 North Cherry Avenue, Tucson, AZ 85721.
[6] Princeton University Observatory, Peyton Hall, Princeton, NJ 08544.
[7] Space Telescope Science Institute, 3700 San Martin Drive, Baltimore, MD 21218.
[8] Max-Planck-Institut für Extraterrestrische Physik, Geissenbachstr. 1, D-85741 Garching, Germany.
[9] Apache Point Observatory, P.O. Box 59, Sunspot, NM 88349-0059.
[10] Department of Astronomy and Astrophysics, University of Chicago, 5640 South Ellis Avenue, Chicago, IL 60637.

TABLE 1
SUMMARY OF CVs WITH SDSS SPECTRA IN 2001

SDSS[a]	Date[b]	g	$u-g$	$g-r$	$r-i$	$i-z$	Comments[c]
J013132.39−090122.3*	Sep 26	18.27	−0.07	−0.14	−0.19	0.16	PB 8928
J013701.06−091234.9*	Aug 26	18.69	0.27	0.23	0.41	0.29	
J031051.66−075500.3*	Jan 15	15.49	0.25	−0.25	−0.15	−0.22	DN
J040714.78−064425.1*	Jan 1	17.75	0.26	0.32	0.36	0.28	Ec
J073817.75+285519.7	Nov 19	19.38	0.45	0.69	0.44	0.29	
J075240.45+362823.2*	Apr 18	17.68	0.22	0.16	−0.04	0.03	He II
J080215.39+401047.2[d]	Oct 19	16.69	0.09	−0.06	0.01	−0.02	NL KUV07589+4019
J080908.39+381406.2	Dec 8	15.61	0.14	−0.03	−0.15	−0.11	He II, SW Sex type
J084400.10+023919.3	Nov 11	18.34	−0.13	0.39	0.38	0.26	
J085107.39+030834.4	Nov 12	18.80	−0.11	−0.07	0.04	0.23	CT Hya
J085344.00+574841.0*	Jan 15	16.39	−0.46	0.34	−0.04	0.22	BZ UMa
J090103.93+480911.1	Nov 25	19.26	−0.07	0.11	0.14	0.14	High i
J092009.54+004244.9*	Jan 20	17.45	0.01	0.13	0.11	0.03	Ec
J093238.21+010902.5*	Feb 25	20.31	−0.58	0.72	0.45	0.01	He II
J094431.71+035805.5	Dec 23	16.80	−0.34	0.60	0.53	0.31	RX J0944.5+0357
J101037.05+024915.0*	Feb 17	20.76	−0.38	0.37	−0.35	0.30	
J102347.67+003841.2*	Feb 1	17.99	1.61	0.56	0.15	0.06	FIRST J102347.6+003841
J113722.25+014858.6*	Mar 21	18.74	−0.08	0.15	0.38	0.59	RZ Leo
J113826.82+032207.1*	Mar 21	14.85	−0.17	−0.28	0.08	0.24	T Leo
J114628.80+675909.7*	Feb 15	18.78	−0.31	−0.09	0.20	−0.02	
J123813.73−033933.0*	Apr 1	17.82	0.06	−0.05	−0.15	−0.07	High i
J124325.92+025547.5*	Apr 25	18.30	−0.24	0.24	−0.01	0.08	
J125023.85+665525.5*	Mar 20	18.70	0.02	0.02	−0.05	0.11	High i
J125834.74+640823.1*	Dec 29	20.55	−0.55	0.39	−0.11	0.16	
J125834.77+663551.6*	Mar 20	20.20	0.07	−0.06	−0.02	0.36	
J132723.39+652854.3*	Mar 20	17.77	0.18	0.12	−0.05	−0.09	Ec, He II, SW Sex type
J144659.95+025330.3*	Apr 28	18.20	−0.25	0.20	0.11	0.06	He II, NP
J145003.12+584501.9*	May 27	20.64	−0.08	0.23	−0.32	−0.03	
J152857.86+034911.7*	Apr 26	19.53	−0.49	0.16	0.18	0.11	
J155331.12+551614.5*	May 27	18.49	1.51	1.06	0.40	1.00	Polar
J163605.01+465204.5	Aug 23	16.72	0.13	−0.13	−0.11	−0.09	
J170053.30+400357.6*	Jan 19	19.43	0.09	0.89	0.45	0.26	Polar
J204448.92−045928.8*	Aug 24	16.86	0.41	0.60	0.27	0.30	
J204817.85−061044.8*	Aug 24	19.35	−0.17	0.10	0.06	0.29	
J205017.84−053626.8*	Sep 24	18.13	−0.27	0.16	0.24	0.39	He II, H, L
J205914.87−061220.5*	Sep 24	18.38	−0.16	−0.01	0.21	0.20	
J210131.26+105251.5	Oct 25	18.08	−0.23	0.01	−0.10	−0.05	He II, H, L
J215411.13−090121.7	Oct 20	19.19	−0.15	0.01	0.05	0.04	
J220553.98+115553.7	Nov 11	20.07	0.30	0.00	−0.18	0.02	
J223439.93+004127.2	Aug 22	18.10	−0.19	0.19	0.13	0.32	
J223843.84+010820.7	Aug 24	18.17	−0.08	−0.04	−0.02	0.03	He II, Aqr 1
J225831.18−094931.7	Dec 15	15.61	−0.30	0.17	−0.02	0.21	PB 7412

[a] Objects marked with an asterisk are publicly available in the SDSS DR1.
[b] UT date of spectrum in 2001.
[c] "DN" is a dwarf nova, "Ec" is eclipsing, "NL" is a novalike, "H" and "L" shows high and low brightness states, and "NP" is not polarized.
[d] Object is northeastern star of a close pair.

objects at zero redshift resulted in the identification of the 42 CVs listed in Table 1. This list includes the objects that will be in Data Release 1 (DR1), as well as several others that were found on additional plates taken in 2001. The magnitudes and colors are from the point-spread function photometry and have not been corrected for reddening. Figure 1 shows the locations of the 42 CVs in SDSS color-color plots along with the stellar locus.

During 2001, we also conducted follow-up observations to refine the nature of the CVs that were being discovered. Photometry was accomplished using the University of Washington 0.76 m telescope at Manastash Ridge Observatory (MRO), using a 1024 × 1024 CCD and a Harris V filter and also with the US Naval Observatory Flagstaff Station (NOFS) 1 m Ritchey-Chrétien telescope, using a 2048 × 2048 SITe/Tektronix CCD. The magnitudes were measured using the IRAF[11] task QPHOT, and a light curve was constructed from differential magnitudes with respect to comparison stars on each frame. In order to obtain the highest time resolution with the NOFS, no filter was used. The NOFS CCD has a wide-band response that falls between Johnson V and Cousins R but is somewhat closer to a V response. From separate nights of calibrated all-sky photometry using Landolt standards, the Johnson B and V

[11] IRAF (Image Reduction and Analysis Facility) is distributed by the National Optical Astronomy Observatory, which is operated by the Association of Universities for Research in Astronomy, Inc., under cooperative agreement with the National Science Foundation.

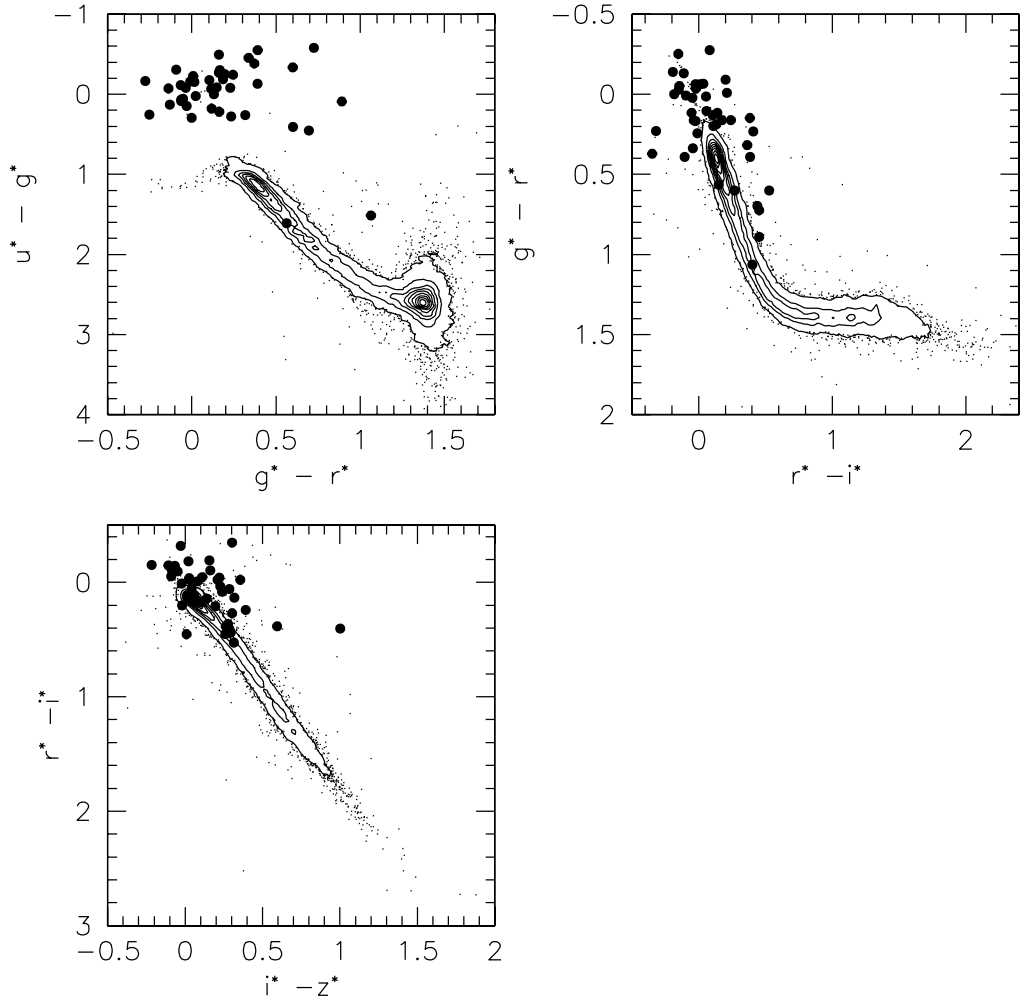

FIG. 1.—SDSS color-color plots of the objects in Table 1. Filled circles are the CVs, and small dots and contours (at intervals of 10% of the peak) are stars defining the stellar locus.

magnitudes of the comparison stars were calibrated and used to place the photometry of the SDSS sources onto the Johnson *V*-magnitude system.

Time-resolved spectroscopy was done at the 3.5 m telescope at Apache Point Observatory (APO) with the Double Imaging Spectrograph in high-resolution mode (resolution about 3 Å) and a 1″.5 slit. Blue and red spectra were obtained on all nights except for 2002 May 9, when only the red spectrograph was available. The reductions were identical to those of Paper I, and details are provided in that reference. For the objects with sufficient time coverage to determine a radial velocity curve, velocities were measured with either the "e" or "k" routines in the IRAF SPLOT package (for simple or narrow line structure) or with the double-Gaussian method (Shafter 1983). Sinusoidal fits to these velocities were then used to determine γ (systemic velocity), K (semiamplitude), P (orbital period), and ϕ_0 (phase of crossing from red to blue).

Additionally, the spectropolarimeter SPOL was used on the 2.2 m telescope at Steward Observatory (SO) to measure the circular polarization of a few sources to determine if they were magnetic CVs. The dates and type of follow-up observations are summarized in Table 2.

3. RESULTS

For convenience, throughout the rest of this paper, we will abbreviate the names to SDSS hhmm (except for the two sources that are identical in the first four coordinates, 1258, so we add the degrees of declination to the name to differentiate the two). The coordinates are accurate enough to identify the objects easily on the Digitized Sky Survey. The few objects that have close companions on the sky are identified as notes to the table. The last column of Table 1 gives a brief comment on any notable properties of the system.

Figure 2 shows the SDSS spectra for all systems. Table 3 lists the equivalent widths and fluxes of the prominent hydrogen Balmer and helium lines, as well as the plate and fiber number of each spectrum. The large strength of He II in some systems allows an automatic separation into those with possible magnetic white dwarfs (see § 3.4). Follow-up observations were targeted first for those systems with prominent He II or with prominent central absorption lines that would signify an eclipsing system. The results for those systems with sufficient data to accomplish a detailed classification are presented below.

TABLE 2
FOLLOW-UP DATA

SDSS	UT Date	Site	Time (UT)	Exp. (s)	Data Obtained
0131	2002 Dec 29	APO	03:35–05:30	600	11 spectra
0137	2003 Jan 4	APO	03:12–05:14	600/900	8 spectra
0310	2001 Sep 19	APO	10:18–11:47	300	13 spectra at outburst
0407	2001 Jan 16	APO	02:30–06:06	600	19 spectra
0407	2001 Sep 17	MRO	10:30–12:37	600	*V* filter photometry
0407	2002 Nov 14	NOFS	04:47–10:18	180	*V* photometry
0407	2002 Dec 13	NOFS	03:13–07:07	120	*V* photometry
0738	2001 Dec 21	APO	10:10–12:20	900	8 spectra
0752	2001 Oct 21	APO	10:23–12:18	900	7 spectra
0809	2002 Jan 9	APO	10:04–12:55	300	27 spectra
0901	2001 Dec 21	APO	07:45–09:58	900	8 spectra
0920	2001 Mar 16	APO	07:48–09:07	600	7 spectra
0920	2003 Feb 7	NOFS	06:18–11:49	120	*V* photometry
0920	2003 Feb 10	NOFS	05:47–11:40	120	*V* photometry
0944	2002 Jan 9	APO	07:37–09:55	300	22 spectra
1023	2001 Dec 10	APO	08:57–10:50	600	10 spectra
1137	2002 May 9	APO	02:58–05:27	600	14 red spectra
1146	2003 Jan 4	APO	10:07–13:09	600/900	11 spectra
1238	2001 Dec 21	APO	12:34–13:01	900/600	2 spectra
1238	2002 Mar 25	APO	05:07–07:00	900	7 spectra
1243	2002 May 9	APO	05:34–07:00	600	8 red spectra
1250	2002 May 9	APO	07:24–09:45	900	10 spectra
1446	2002 May 11	SO	07:22–08:12	3000	Spectropolarimetry
1446	2002 Jun 15	APO	05:37–06:45	600	6 spectra
1636	2002 Jul 16	MRO	06:33–10:23	600	*V* filter photometry
1700	2001 Aug 7	MRO	04:33–06:55	600	*V* filter photometry
1700	2001 Aug 9	MRO	04:25–07:17	600	*V* filter photometry
1700	2001 Aug 15	MRO	04:25–08:54	600	*V* filter photometry
1700	2001 Oct 17	APO	02:32–03:20	900/1200	2 spectra
1700	2002 May 9	APO	09:51–11:04	600	7 red spectra
1700	2002 May 11	SO	09:17–11:12	900	Spectropolarimetry
2050	2002 Sep 7	MRO	04:00–06:19	600	*V* filter photometry
2050	2002 Sep 27	APO	04:47–06:36	900	7 spectra
2101	2002 Oct 3	APO	05:07–06:26	600/900	6 spectra
2234	2003 Jan 4	APO	01:05–03:02	600	11 spectra
2238	2003 Sep 8	MRO	06:44–10:29	600	Unfiltered photometry
2238	2002 Dec 29	APO	01:44–03:29	600/900	7 spectra

3.1. *Previously Known Systems*

Spectra of the dwarf novae CT Hya (SDSS 0851), RZ Leo (SDSS 1137), T Leo (SDSS 1138), and BZ UMa (SDSS 0853), which are all cataloged in the Downes et al. (2001) catalog (D01), were obtained as a result of the color selection algorithms. The spectra of CT Hya, T Leo, and BZ UMa show the typical characteristics of quiescent dwarf novae that are dominated by their accretion disks (i.e., prominent Balmer and He I emission lines and Ca emission in the near IR). RZ Leo, on the other hand, shows strongly doubled lines and broad absorption surrounding the emission lines, which indicates the white dwarf, rather than an accretion disk, is contributing much of the blue light. Mennickent & Tappert (2001, hereafter MT01) have recently identified a spectroscopic orbital period of 1.84 hr and comment on the large V/R variations throughout the orbit. They measured the velocities using a single Gaussian fit to the entire line that resulted in a noisy radial velocity curve. Since the lines are clearly not Gaussian (Fig. 3), we attempted a better solution by using the double-Gaussian method on the line wings, using the MT01 period. With a Gaussian width of 100 km s^{-1} and a separation of 2000 km s^{-1}, our solution results in a larger K amplitude (Table 4) and a smoother radial velocity curve (Fig. 4).

SDSS 0944.—The *ROSAT*-identified CV RX J0944.5+0357 (Jiang et al. 2000, hereafter J00), which is SDSS 0944, was also in the Sloan spectroscopic coverage. However, the SDSS spectrum (Fig. 2) taken in 2001 December shows that the flux at 5500 Å is 2.5 times lower (1 mag) than in the J00 observations (1999 January). This is consistent with the magnitude differences in the two data sets (J00 give a B magnitude of 16.1, whereas the SDSS photometry is 17.0 in g). The lower flux results in changes in the line emission and the domination of the secondary over the accretion disk in the red (see § 3.5). Since both the Hamburg survey and the USNO-A2.0 magnitudes are consistent with the brighter fluxes, while the SDSS and APO spectra are consistent with the fainter magnitudes, this system either has large variations of mass transfer on long timescales or a large orbital flux variation. The follow-up APO time-resolved spectra over 2.3 hr show a 1 mag change in the continuum over this interval (Fig. 5), which argues for an orbital variation. The radial velocity curve curves of both Hβ and Hα (Fig. 6,

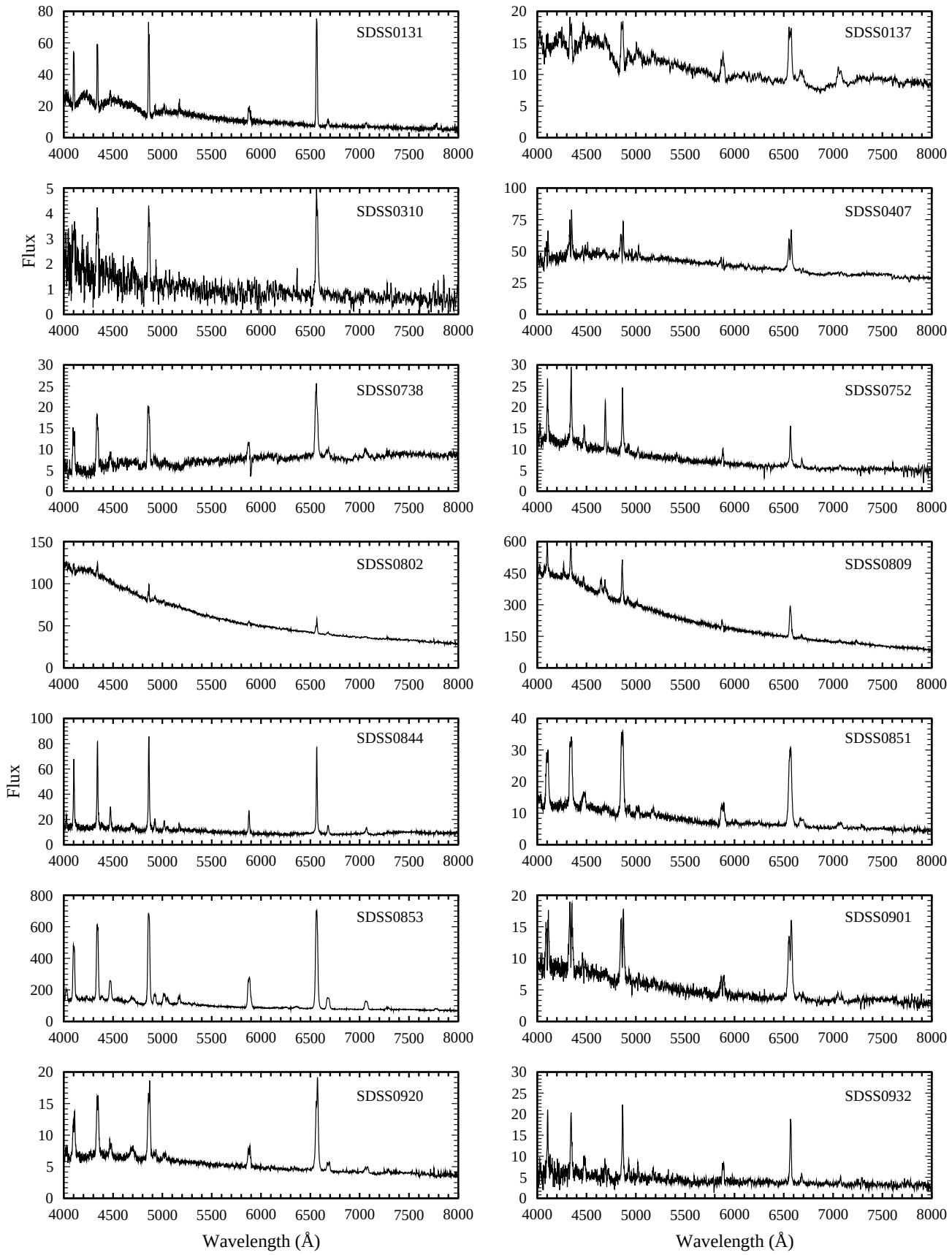

FIG. 2.—SDSS spectra of the newly discovered CVs in the interval from 4000–8000 Å. The flux scale is in units of flux density 10^{-17} ergs cm^{-2} s^{-1} Å^{-1}.

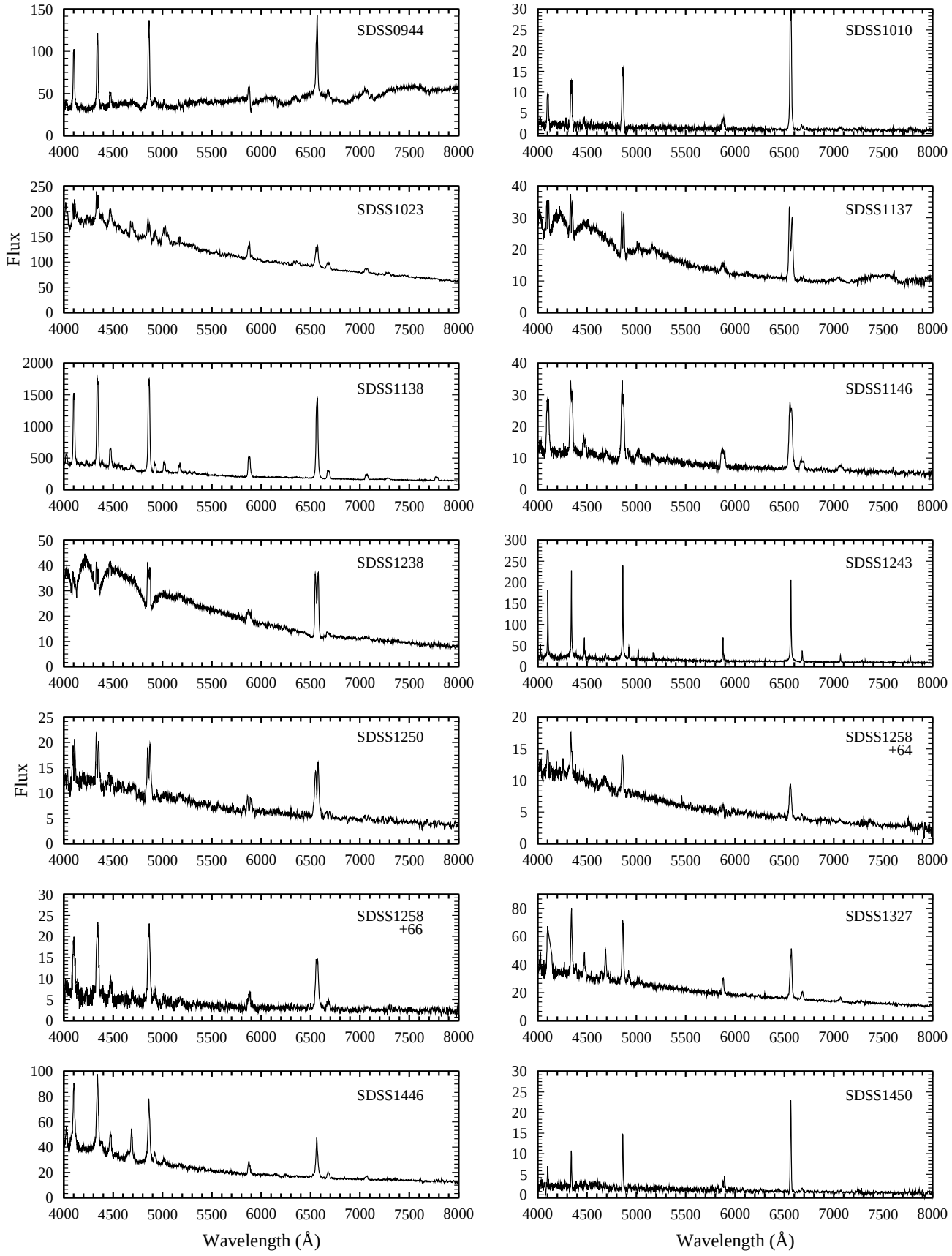

FIG. 2.—*Continued*

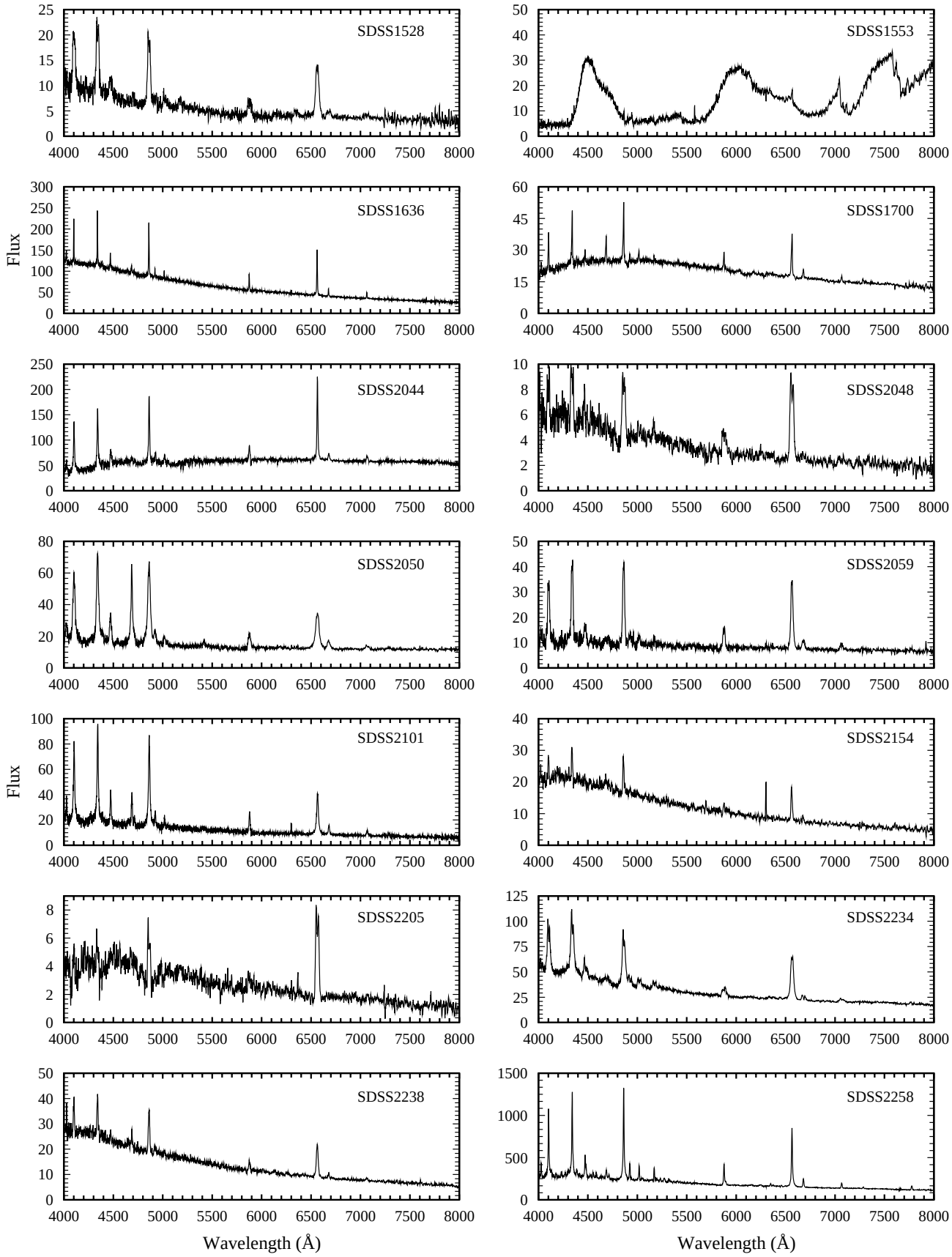

FIG. 2.—*Continued*

TABLE 3
SDSS Spectral Line Fluxes and Equivalent Widths[a]

		Hγ		Hβ		Hα		He 4471		He II 4686	
SDSS	Plate, Fiber	*F*	EW	*F*	EW	*F*	EW	*F*	EW	*F*	EW
0131	662, 384	4.7	25	5.9	44	9.2	147	0.6	2	...	...
0137	662, 552	1.5	12	2.3	21	3.4	38	0.4	3	...	...
0310	459, 222	0.5	31	0.6	50	1.1	138	...	...	...	...
0407	465, 226	8.1	18	5.8	12	10.7	30	...	...	...	...
0738	754, 34	3.3	65	3.5	56	4.9	57	0.5	9	...	...
0752	543, 65	2.8	24	2.4	26	2.0	35	0.7	6	1.4	14
0802	544, 423	1.7	2	2.0	2	2.8	7	...	...	...	...
0809	758, 570	24	6	30	9	35	24	3.8	1	16	5
0844	564, 197	9.6	73	10	88	9.4	101	2.3	18	0.7	6
0851	565, 359	7.5	62	8.7	87	9.0	141	1.5	12	...	...
0853	483, 332	108	76	143	124	171	195	31	22	11	9
0901	764, 589	3.1	37	3.8	58	5.2	143	0.3	4	...	...
0920	473, 98	2.4	35	3.0	46	4.1	91	0.5	7	0.7	10
0932	475, 66	2.4	42	2.6	52	2.7	72	0.7	12	0.5	9
0944	570, 512	16	47	18	50	19	39	2.8	8	...	...
1010	502, 444	1.9	104	2.7	186	5.8	553	0.3	18	...	...
1023	272, 461	16	9	8.3	6	13	14	8.7	5	7.8	5
1137	513, 70	2.6	10	3.5	20	8.3	78	...	...	...	...
1138	513, 562	288	72	327	111	322	173	65	18	21	7
1146	492, 454	7.2	62	7.7	80	8.2	120	1.5	13	0.5	5
1238	335, 85	2.0	6	4.8	20	9.8	84	0.5	1.3	...	...
1243	522, 325	21	89	23	114	23	169	4.3	21	1.2	6
1250	495, 238	2.3	18	3.6	39	4.6	85	0.6	5	...	...
1258+64	602, 264	1.1	10	1.2	14	1.4	32	...	0.4	5	...
1258+66	495, 148	5.4	99	5.1	111	4.3	141	1.2	24	0.4	10
1327	496, 83	7.0	31	6.9	32	6.4	51	2.9	13	4.0	18
1446	537, 454	17	44	12	42	7.7	46	3.9	11	7.0	23
1450	610, 349	0.7	36	1.5	100	2.6	346	...	...	...	...
1528	592, 601	4.2	46	4.2	60	4.1	98	1.0	12	...	...
1553	619, 437	...	...	...	0.1	3	...	...	...	...	...
1636	627, 479	8.0	7	8.9	10	11	24	2.4	2	1.1	1
1700	633, 574	2.5	10	2.9	12	2.8	16	0.4	1.6	4.0	1
2044	635, 387	17	36	17	30	23	37	3.6	7	...	...
2048	635, 127	0.9	16	1.8	42	2.7	103	0.2	3	...	...
2050	636, 331	17	95	18	109	11	83	3.3	20	11	70
2059	636, 599	8.1	76	7.9	79	7.8	101	1.9	18	...	...
2101	727, 324	14	66	12	65	8.2	90	3.6	21	3.7	23
2154	716, 299	1.3	6	1.8	11	1.7	21	...	0.4	2	...
2205	734, 30	0.5	13	1.0	38	2.3	136	...	...	...	...
2234	376, 631	20	40	20	55	16	68	2.4	5	...	...
2238	377, 540	2.1	8	2.6	13	3.1	34	0.3	1.5	0.7	3
2258	725, 306	122	42	137	52	100	61	35	13	12	5

[a] Fluxes are in units of 10^{-15} ergs cm^{-2} s^{-1}, and equivalent widths are in units of angstroms.

Table 4) indicate an orbital period near 3.25 hr, but a longer data set will be needed to pin this down precisely. It is unusual to have an object in the 3–4 hr period range that has a low enough $\dot{M}$ to show the underlying stars, since most systems in this period range are high mass transfer objects with prominent accretion disks (Warner 1995). In addition, the shape and phasing of the continuum light curve (Fig. 5) is inconsistent with either an eclipse (which would have minimum light near phase 0) or a hot spot coming into view (which would have maximum light near phase 0.8). Clearly, further data on this system are needed.

SDSS 1023.—The recently identified FIRST source J102347.6+003841 (Bond et al. 2002) is also among the SDSS spectra of 2001 (SDSS 1023). Since only magnetic CVs have shown radio emission, this is an excellent candidate for a polar (a spin-orbit synchronized AM Her system with magnetic field over 10 MG) or an intermediate polar (IP) system with a field near 1 MG and a spin period for the white dwarf much less than the orbital period. Our 10 APO spectra obtained over 1.7 hr show the double-peaked profile mentioned by Bond and a changing intensity of He II. The velocity curve (Fig. 7 and Table 4) indicates the orbital period is about 3 hr, and the high semiamplitude for Hβ is typical of a polar. While the period is consistent with either an IP or a polar, the emission lines are more compatible with an IP interpretation, since they do not show the large equivalent widths nor the narrow components that are typically seen in polars, especially the component from the irradiated secondary, which usually is strongest near phase 0.5. Although Bond et al. (2002) could not identify the spin period of the white dwarf from their photometry, it could be shorter than their time resolution. Further spectroscopy

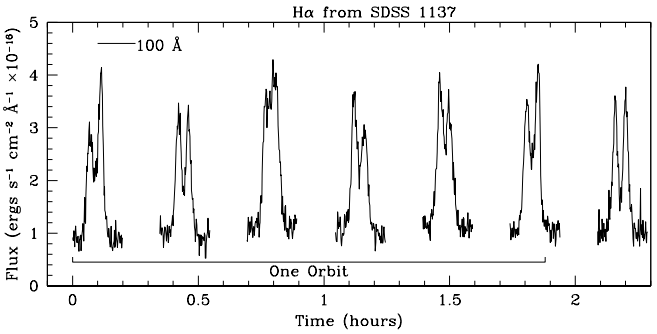

FIG. 3.—Time-resolved APO spectra of RZ Leo (SDSS 1137), showing the large changes in the blue and red components of Hα throughout the orbit.

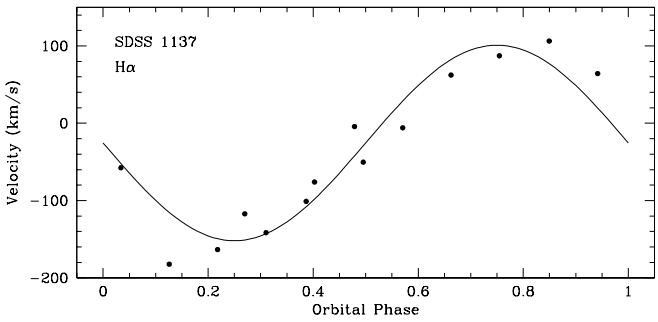

FIG. 4.—Radial velocity data of RZ Leo obtained from using a double-Gaussian fitting to the line wings, with the best-fit solution from Table 4 shown as the solid curve.

throughout the entire orbit, as well as spectropolarimetry, should resolve the issue.

SDSS 2238.—The source listed as Aqr1 in D01 and labeled as a CV, based on its identification from the Berg et al. (1992) quasar survey, also was color-selected (SDSS 2238). This object shows He II in both the SDSS and Berg et al. (1992) spectra and could be a magnetic CV candidate. APO spectra show an orbital period of 2.0 hr from the velocities (Fig. 8 and Table 4), but the 3.75 hr of MRO photometry (Table 2) shows only random variability at the 0.2 mag level, with no large periodic variability as is typical for polars. Polarimetry will be needed to check the magnetic nature.

There are also three sources that appear in past surveys but which were not previously identified as CVs.

SDSS 0131.—SDSS 0131 was identified as a blue object (PHL 3388, PB 8928) in the survey of Berger & Fringant (1984, hereafter BF84). Its SDSS spectrum shows strong emission lines surrounded by broad absorption, so that it is likely a system with a low disk contribution (see § 3.5 below). The 2 hr of follow-up spectra with APO indicate an orbital period of 1.6 hr (Table 4; Fig. 9), which is consistent with a low mass transfer rate.

SDSS 0802.—The coordinates of SDSS 0802 match those of KUV 07589+4019, which was identified as an sdB star by Wegner & Boley (1993). However, the spectrum previously obtained lacked the signal-to-noise ratio and resolution to

TABLE 4
RADIAL VELOCITY SOLUTIONS

SDSS	Line	P (minutes)	γ	K (km s^{-1})	T_0 (JD 2,450,000+)	σ	Method[a]
0131	Hβ	98	−63 ± 1	29 ± 5	2,637.694	11	dG (1400)
0131	Hα	98	50.1 ± 0.3	25 ± 2	2,637.696	5	dG (1400)
0137	Hβ	86	21 ± 2	118 ± 13	2,643.687	16	dG (1300)
0137	Hα	80	48 ± 2	98 ± 8	2,643.673	14	dG (1500)
0407	Hβ	238	85 ± 2	122 ± 15	1,925.602	37	dG (1700)
0407	Hα	238	77 ± 4	69 ± 29	1,926.618	72	dG (1400)
0738	Hβ	127	75 ± 16	176 ± 43	2,264.916	51	e
0738	Hα	125	84 ± 12	264 ± 74	2,264.962	100	e
0752	Hβ	162	3 ± 8	78 ± 15	2,203.848	21	dG (300)
0809	Hβ	143	−14 ± 1	128 ± 9	2,283.967	28	dG (1000)
0809	Hα	143	109 ± 1	84 ± 14	2,283.977	45	dG (900)
0944	Hβ	195	11 ± 3	69 ± 5	2,283.869	19	e
0944	Hα	195	87 ± 5	119 ± 11	2,283.850	37	e
1023	Hβ	182	−194 ± 14	190 ± 18	2,253.841	36	e
1023	Hα	182	−4 ± 16	84 ± 24	2,253.861	40	e
1137	Hα	113	−25 ± 2	126 ± 12	2,403.677	30	dG (2000)
1146	Hβ	99	−24 ± 2	120 ± 18	2,643.960	38	dG (2100)
1146	Hα	95	−2.8 ± 0.2	69 ± 14	2,643.964	31	dG (2000)
1238	Hβ	76	−32 ± 10	202 ± 41	2,358.708	68	e
1238	Hα	76	−65 ± 2	93 ± 9	2,358.705	15	e
1700	Hα	115	−66 ± 3	89 ± 6	2,403.899	6	e
2050	Hα	138	86 ± 3	38 ± 12	2,544.748	18	e
2234	Hβ	120	−19.6 ± 0.3	65 ± 4	2,643.524	7	dG (1500)
2234	Hα	124	23.5 ± 0.3	108 ± 4	2,643.523	8	dG (1900)
2238	Hβ	121	−134 ± 6	99 ± 14	2,637.613	21	dG (1300)
2238	Hα	121	−91 ± 16	147 ± 33	2,637.625	29	dG (2200)

[a] In this table, "dG" refers to double Gaussian (value in parenthesis is separation in kilometers per second) and "e" refers to the centroid in SPLOT.

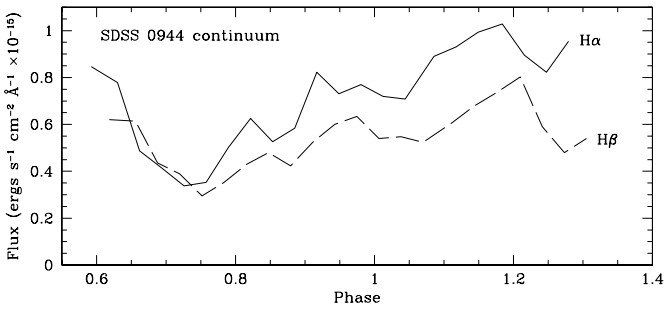

FIG. 5.—Blue and red continuum changes in SDSS 0944 throughout the orbit as evident from APO spectra.

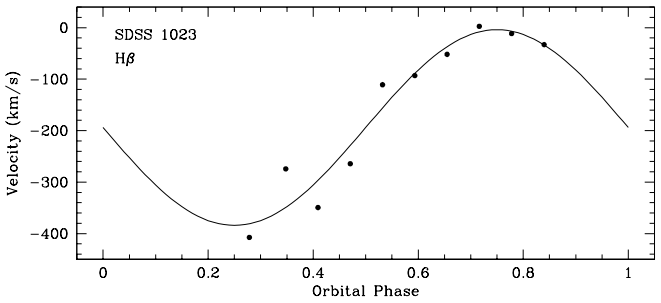

FIG. 7.—Velocity curve of SDSS 1023 with the best-fit sinusoid superposed.

detect the Balmer and He I emission lines evident in the SDSS spectrum (Fig. 2). Thus, this object is likely to be a low-inclination, high mass transfer rate novalike system with a bright accretion disk.

SDSS 2258.—SDSS 2258 was also previously identified as a blue star (PB 7412) in the BF84 survey and then classified as an emission-line object in the HK survey of Beers et al. (1996). Its coordinates are close (within an arcminute) to the X-ray source RX J225834.4−094945, although this does not guarantee they are the same object. The SDSS spectrum shows a strong, narrow emission line source that is typical of a low-inclination CV.

3.2. *High-Inclination Systems*

The systems with high inclination usually show very prominent central absorption in the Balmer lines with increasing absorption up the Balmer series. The CVs in Figure 2 that show this effect are SDSS 0407, SDSS 0901, SDSS 1137, SDSS 1238, SDSS 1250, and SDSS 1327. Photometry of SDSS 1137 (RZ Leo) by Howell & Szkody (1988) and MT01 has shown a large orbital modulation but no eclipses. Follow-up photometry on SDSS 0407, SDSS 0920, and SDSS 1327 reveals eclipses in these three systems, while time-resolved spectroscopy provides the radial velocities, as well as the periods (Tables 2 and 4). The most extensive observations exist for SDSS 1327 (which are described in a separate paper; Wolfe et al. 2003) and SDSS 0407.

SDSS 0407.—MRO photometry first revealed a deeply eclipsing (2 mag) system, but clouds prevented the acquisition of further data. NOFS observations later obtained two eclipses (Fig. 10) that revealed an orbital period of 3.96 hr and a strong orbital hump modulation due to a prominent hot spot. APO spectra were obtained for 3.5 hr, covering an eclipse. Figure 11 shows the typical double-peaked profile at phase 0.5, the strong blue peak during the hump phases and the remaining Balmer emission during the eclipse itself. Using the photometric eclipse period, the double-Gaussian fitting applied to the Balmer lines gave a good fit for Hβ but large errors for Hα. The resulting parameters from the sine fit to the velocities are given in Table 4, and the velocity curve for Hβ is shown in Figure 12.

SDSS 0920.—NOFS photometry revealed eclipses for this system even though the lines do not show the usual deep doubling. Figure 13 shows the 2 mag deep eclipses recurring on an orbital period of 3.6 hr. Unlike SDSS 0407, there is no strong modulation hump from a hot spot. Since the APO spectra cover less than half an orbit, a reliable radial velocity solution could not be determined.

SDSS 1238.—The double-Gaussian fitting to the complex line profiles of this source enabled a period determination of 1.27 hr from both the Hα and Hβ lines (Fig. 14). The very short period and the appearance of the spectra are very similar to low mass transfer systems, such as WZ Sge and RZ Leo.

SDSS 1250.—The 2.3 hr of APO time-resolved spectra indicate an orbital period near 5.6 hr but further data are needed to confirm this result. There was no noticeable eclipse within our spectral coverage, but the long (15 minutes) integration times and incomplete coverage of the

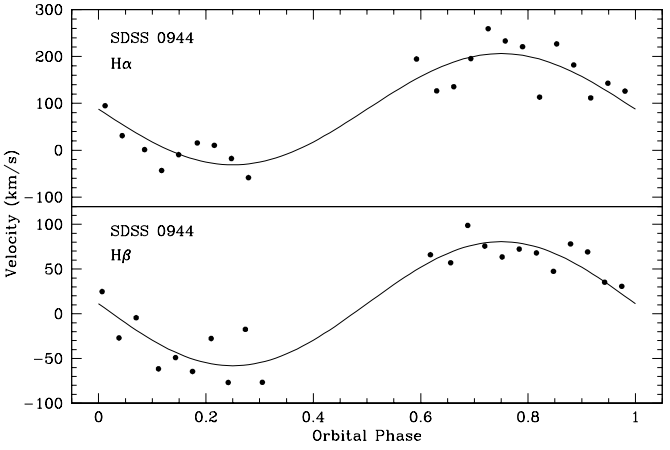

FIG. 6.—Velocity curves of SDSS 0944 with the best-fit sinusoids (Table 4) plotted on the data.

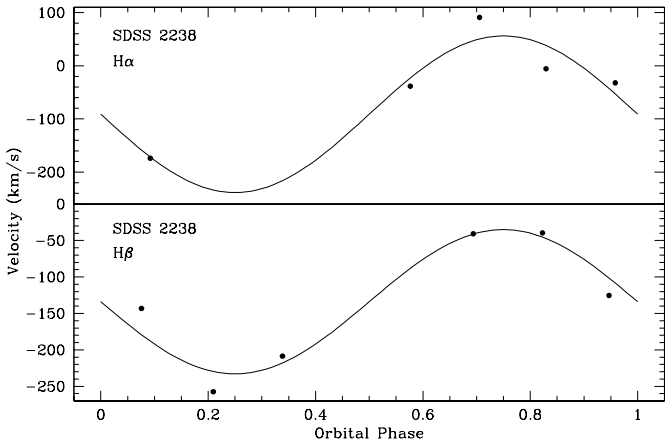

FIG. 8.—Same as Fig. 7, but for SDSS 2238

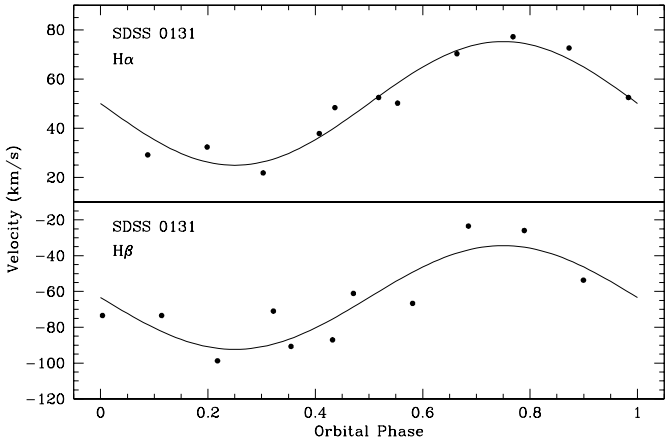

FIG. 9.—Same as Fig. 7, but for SDSS 0131

orbit do not allow us to eliminate their existence. Photometry with better time resolution is needed to search for possible eclipses.

3.3. *Dwarf Novae*

As mentioned in Paper I, there are three epochs of observation for all SDSS spectral sources to determine if there are large magnitude changes related to a dwarf nova outburst or to changes from low to high mass transfer states in novalikes. These include the SDSS photometric epoch, the SDSS spectral epoch, and the Digitized Sky Survey (DSS) epoch. A dwarf nova outburst can be distinguished from the high state of a novalike by the spectral appearance, since a dwarf nova at outburst shows broad absorption lines (from the thick disk), while a novalike at a high state usually shows an enhancement of all emission, especially the high excitation lines of He II (Warner 1995).

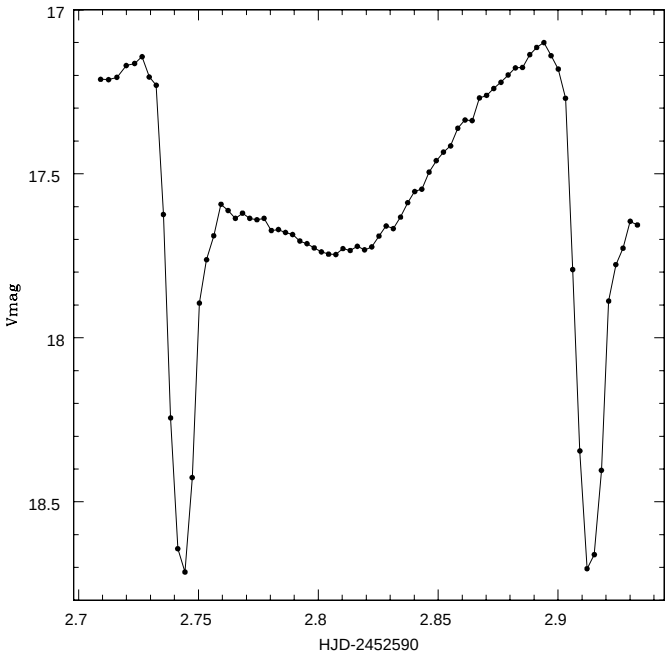

FIG. 10.—NOFS light curve of SDSS 0407, showing the deep eclipse and prominent orbital hump.

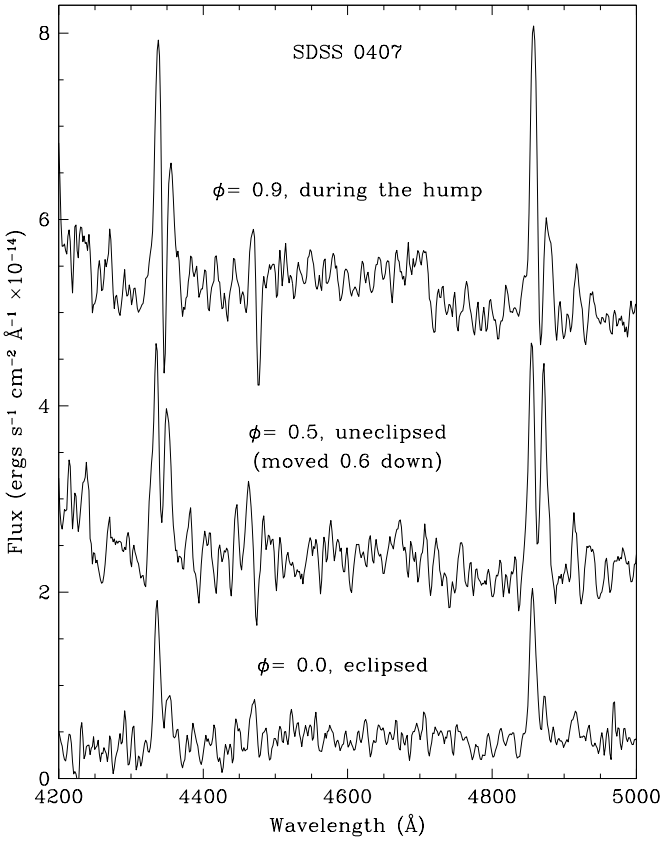

FIG. 11.—APO spectra showing the eclipse, hump, and uneclipsed phases of SDSS 0407.

SDSS 0310.—Of the objects in Table 1, we can identify SDSS 0310 as a bona fide dwarf nova, since the SDSS photometry and the APO follow-up spectra caught it at outburst (Fig. 15), while the SDSS spectrum (Fig. 2) was at quiescence. Photometry by A. Henden (2003, private communication) has determined a quiescent magnitude of $V = 20.7$. Unfortunately, follow-up APO spectra at quiescence were too noisy to allow a good radial velocity solution, and we could not obtain a good solution from the broad absorption lines at outburst either, so we have no estimate of the orbital period.

Three additional systems (SDSS 1146, SDSS 1636, and SDSS 2234) show typical spectra of dwarf novae, although photometry/spectroscopy during an outburst is needed to confirm the spacing and amplitude of outbursts.

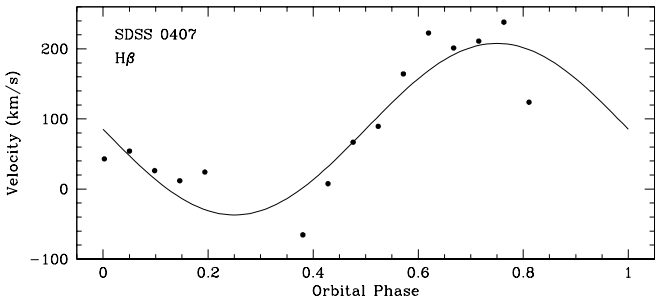

FIG. 12.—Velocity curve of SDSS 0407 with the best-fit sinusoid

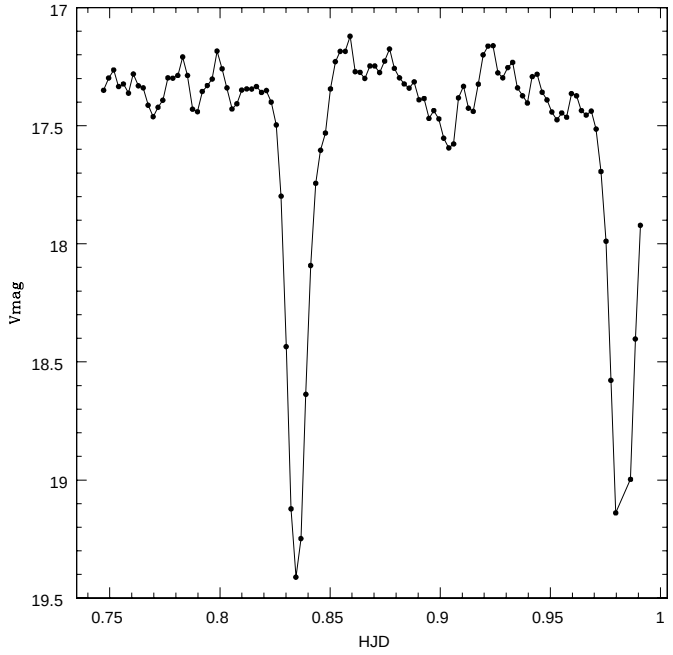

FIG. 13.—Same as Fig. 10, but for SDSS 0920, showing its deep eclipses.

SDSS 1146.—The fit to the velocities derived from APO spectra (Table 4) reveal an orbital period near 1.6 hr (Fig. 16). The short orbital period and large Hβ equivalent width are indicative of a low mass transfer system (Patterson 1984).

SDSS 1636.—The lack of any orbital variation during 4 hr of photometry on SDSS 1636 (Table 2) indicates this is likely a low-inclination system. Time-resolved spectra should be able to reveal the orbital period.

SDSS 2234.—The APO spectra reveal an orbital period of 2.0 hr (Table 4 and Fig. 17) for this system, which places it right at the lower edge of the period gap. The strong blue continuum and emission lines are typical of accretion disk systems.

Two other systems show evidence of low states (SDSS 2050 was observed to be much fainter than its SDSS photometry during MRO observations in 2002 July, and SDSS 2101 is fainter on the DSS than during SDSS observations). The presence of low states together with strong He II emission makes both of these likely candidates for magnetic CVs (see next section). However, sufficient follow-up data are not yet available to confirm the nature of these sources.

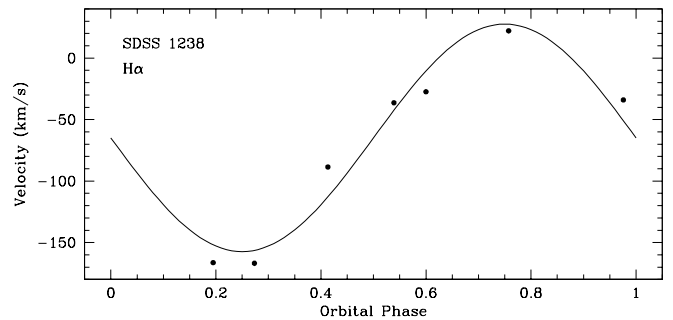

FIG. 14.—Same as Fig. 12, but for SDSS 1238

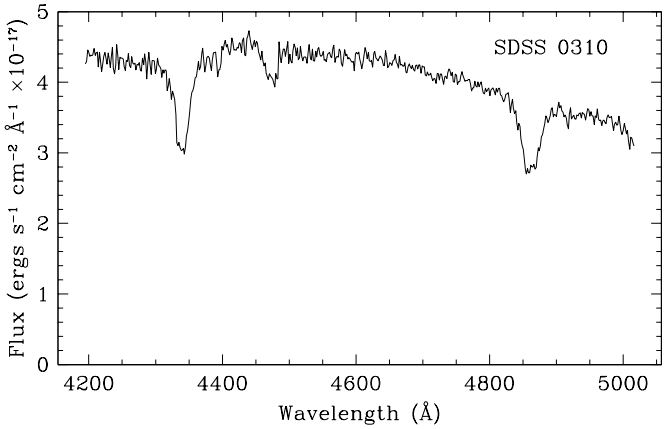

FIG. 15.—APO outburst spectrum of SDSS 0310

3.4. *Novalikes with Strong* He II

The presence of strong He II emission lines often signifies a magnetic white dwarf, since they arise from the ionization of the accretion column(s) by the EUV continuum of a radial accretion shock. If an object shows a large circular polarization and strong modulation of the lines and continuum at the orbital period, it can be classified as a polar. If it shows little or no polarization, generally single-peaked lines, and periodicity at plausible spin timescales of the white dwarf (minutes), it is considered an IP or SW Sex star (some SW Sex stars have recently been proposed as IPs; Rodriguez-Gil et al. 2001).

Figure 2 and Table 3 contain nine systems that clearly have stronger He II lines than are expected for a non-magnetic disk system. These, which we identify as the best candidates for magnetic systems, include SDSS 0752, 0809, 1023, 1327, 1446, 1553, 1700, 2050, and 2101. SDSS 0932 and 2238 may also qualify. Of this group, SDSS 1553 has been identified as an extremely low mass accretion rate polar (Szkody et al. 2003), and as mentioned above, Bond et al. (2002) have identified SDSS 1023 as a FIRST radio source with high probability of being a magnetic IP system. SDSS 1327 is classified as a likely SW Sex star through the work of Wolfe et al. (2003). Our follow-up observations with APO, MRO, and spectropolarimetry at SO have

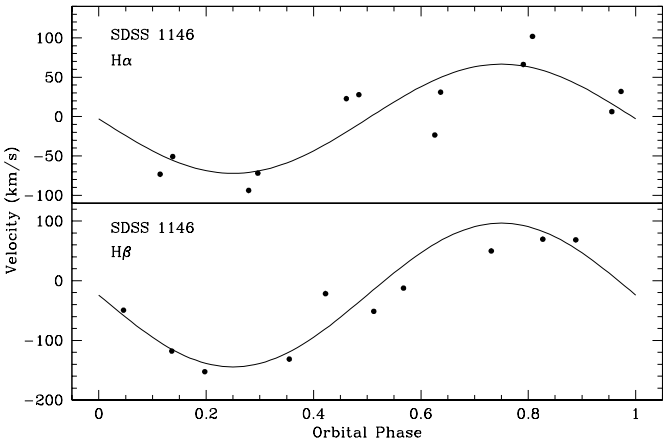

FIG. 16.—Velocity curves of SDSS 1146 with the best-fit sinusoids superposed.

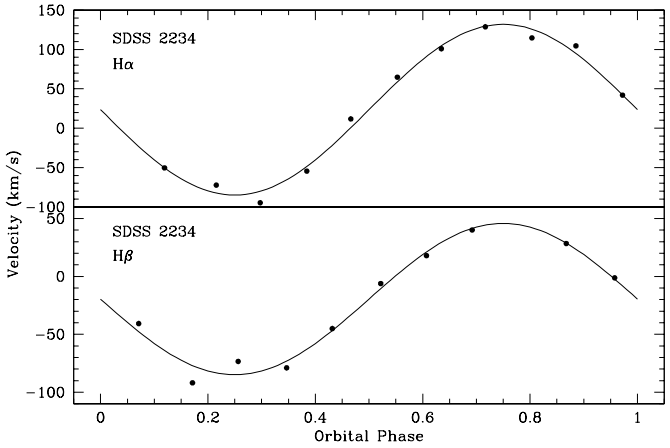

FIG. 17.—Same as Fig. 16, but for SDSS 2234

helped to pin down the nature of a few others. These characteristics are summarized below.

SDSS 1700.—Photometry of SDSS 1700 from MRO (Fig. 18) reveals a strongly modulated light curve with a period of 115 minutes, suggestive of a polar. APO spectra over half the orbit give a radial velocity solution (Table 4) with a relatively low K of 90 km s^{-1} (Fig. 19). Spectropolarimetry at the 2.3 m Bok telescope (Fig. 20) confirms the polar nature, with the broadband circular polarization varying between +2% and +28% over the 2 hr period of the observations. The constant sign of circular polarization indicates that we see only one accretion pole through the orbit, while the rather weakly modulated Hα flux and

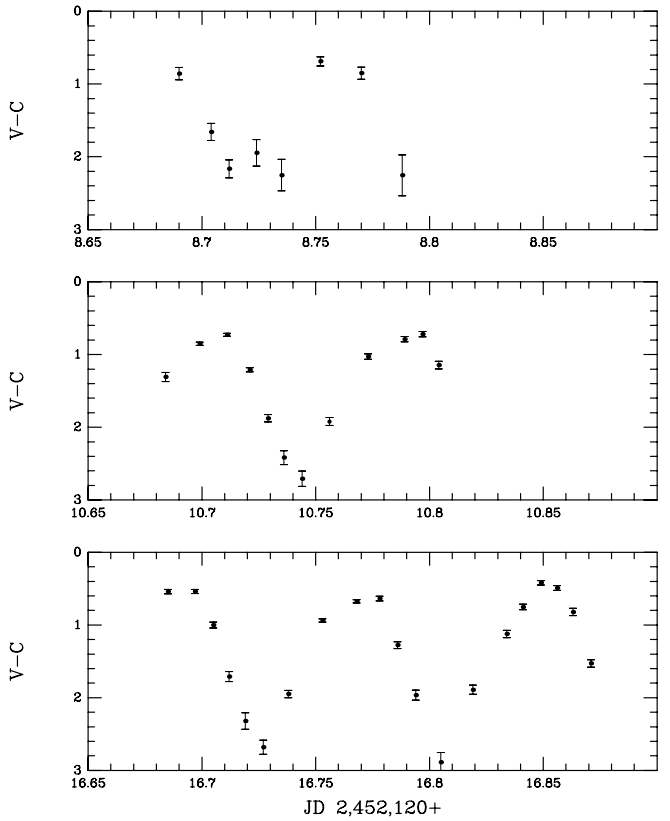

FIG. 18.—MRO differential light curves of SDSS 1700

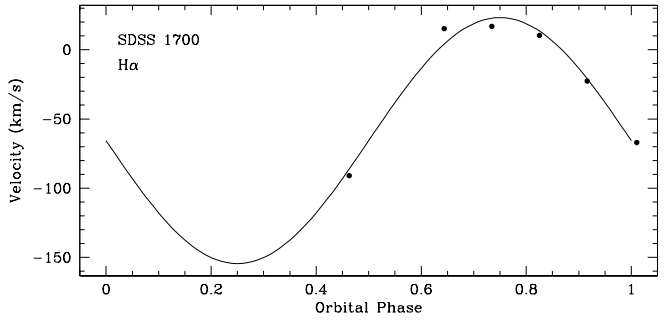

FIG. 19.—Velocity curve of SDSS 1700 with the best-fit sinusoid found by using the photometric period.

modest radial velocity amplitude suggest a rather low inclination. In Figure 20, it is clear that the light-curve variation is due to a changing continuum shape, from rising slightly to the blue in the first spectrum to being strongly convex upward for the next few observations and returning to the initial shape by the end of the sequence. Because these variations correlate with the changing circular polarization, both are taken to arise from the beaming pattern of cyclotron emission. In the co-added polarization spectrum (Fig. 21), diffuse absorption features can be recognized near 6100 Å and between Hβ and He II λ4686. Interpreting these as Zeeman features of Hα and Hβ, respectively, the field strength near the accretion shock is ~30 MG, so the optical spectrum is sampling cyclotron harmonics ~5–9. These characteristics are rather typical for polars.

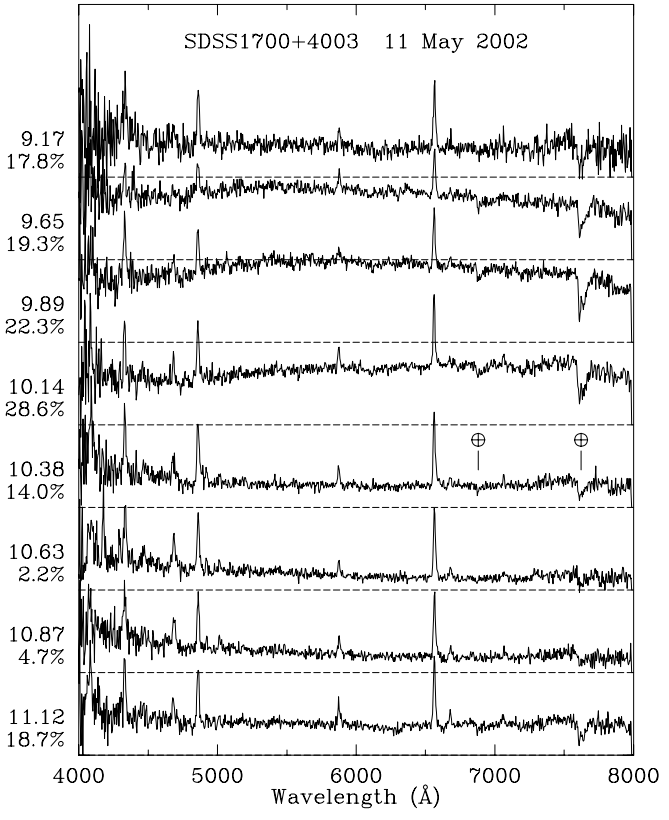

FIG. 20.—Sequence of low-resolution (~13 Å) spectroscopy covering one period of SDSS 1700. The UT and broadband ($\lambda\lambda$4500–7500 Å) circular polarization are listed for each panel at the left.

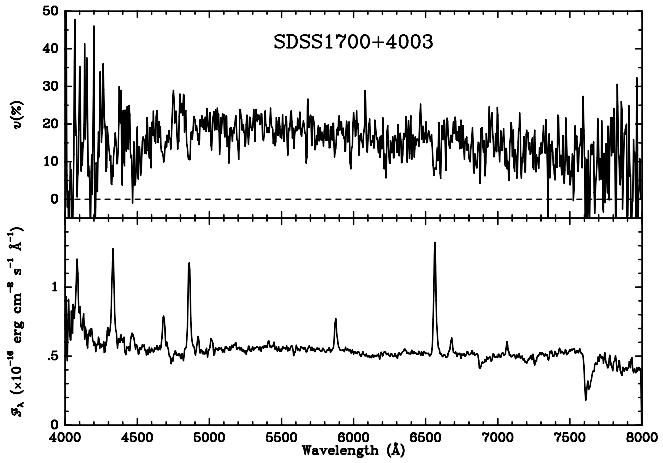

FIG. 21.—Co-added circular polarization (*top*) and spectral flux (*bottom*) for SDSS 1700.

SDSS 0752.—Photometry obtained at NOFS coincident with our recent *XMM-Newton* observation of this source revealed an orbital period of 2.7 hr (A. Henden 2003, private communication). The 1.9 hr of APO time-resolved spectra show velocity variations on this period (Fig. 22). The spectra show the usual narrow and broad components associated with a polar system, so it is very likely that this object will show some polarization. Further discussion on this source will be deferred until the analysis of the *XMM-Newton* results are completed.

SDSS 0809.—The time-resolved spectra over almost 3 hr clearly identify an orbital period of 2.4 ± 0.1 hr in this system (Fig. 23). Although this is slightly shorter than the nominal 3–4 hr range typical of SW Sex stars, the spectra show the strong modulation and usual signature of deep absorption (especially in the He I and Balmer lines) near phase 0.5 (Fig. 24). Since there is no apparent eclipse, this system may be one of the lower inclination SW Sex systems.

SDSS 1446.—Spectropolarimetry at SO established a polarization limit of $+0.38\% \pm 0.27\%$ for SDSS 1446, indicating that this system cannot be a polar. The APO coverage was limited by weather to only slightly more than an hour, so further data are needed to establish the exact nature of this system.

SDSS 2050.—While the 1.8 hr of APO spectra on 2002 September 27 indicate an orbital period near 2 hr, MRO photometry on September 7 only shows an overall declining brightness with some superposed variability during a 2.3 hr observation interval. As noted in the previous section, SDSS

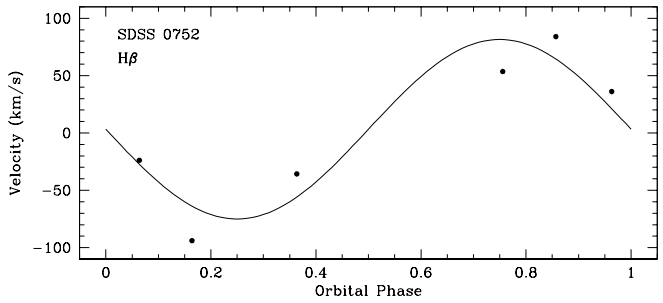

FIG. 22.—Velocity curve of SDSS 0752 with the best-fit sinusoid

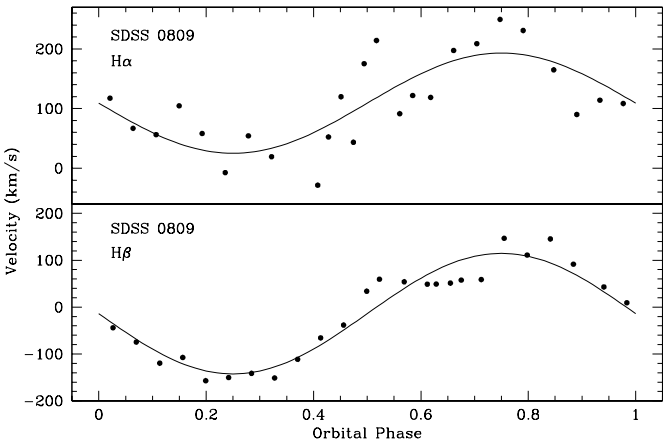

FIG. 23.—Velocity curves of SDSS 0809 with the best-fit sinusoids

2050 was observed to be in a much fainter state (too faint for data acquisition) in 2002 July, so the September variability may be related to a transition state between high and low mass transfer or to orbital variability. Further photometric, spectroscopic, and polarimetric data will be needed to sort out the nature of this object.

SDSS 2101.—While the Balmer lines are very strong in this system and velocities could be easily measured, there was no obvious variation (within 30 km s^{-1}) during the 1.3 hr of APO spectra. Further data will be needed to determine

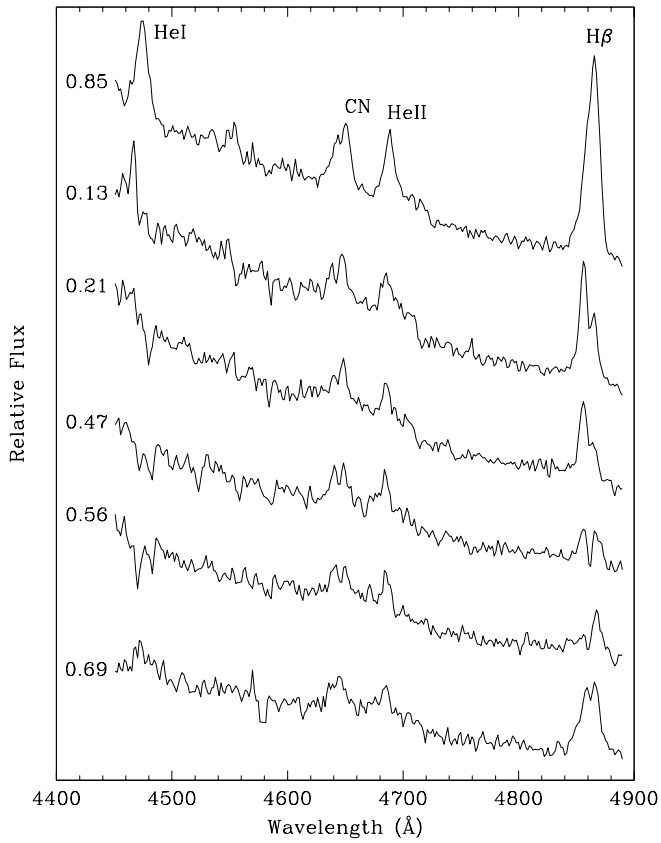

FIG. 24.—Time-resolved spectra of SDSS 0809 showing the changing line structure and deep absorption apparent in the Balmer and He I lines during phases 0.21–0.56. Flux scale is in F_λ units with each successive spectrum offset for clarity.

the orbital period, but it is apparently not a short-period system.

3.5. *Systems Showing the Underlying Stars*

Six systems (SDSS 0131, 0137, 1137, 1238, 2048, and 2205) show broad absorption surrounding the emission lines of Hβ and higher members of the Balmer series. Of these, two (SDSS 0137 and SDSS 1137) also show the TiO bandheads of an M dwarf secondary. These are indicative of the lowest mass transfer systems, where the disk is so tenuous that the underlying stars provide most of the luminosity. Two of the six (SDSS 1137 and 1238) are also high-inclination candidates from their deeply doubled lines (see above). In these cases, the lower disk luminosity may be partly due to the inclination effect, since a disk seen edge on contributes less light than when the entire disk is visible.

Since it is also possible for a dwarf nova on the decline from outburst to show similar absorption features, we checked the spectral fluxes against the SDSS photometry. There is no large difference for any of these systems, so we think the spectra are the normal quiescent states of these systems.

SDSS 0137.—Our 2 hr of spectral coverage of this source shows an ultrashort orbital period of 1.4 hr and a high-amplitude velocity curve (Fig. 25 and Table 4). This is consistent with a very low mass transfer rate system at relatively high inclination.

There are three other systems that show evidence of the secondary star from an upturn in the red portion of the spectrum and the presence of the TiO bandhead at 7100 Å, but no evidence of the white dwarf. These are SDSS 0844, SDSS 0944 (RX J0944.5+0357), and SDSS 1553. The weakness of the features in SDSS 0844 and the strong blue continuum indicates that the disk is still dominant in this system. SDSS 1553 is the very low accretion rate polar mentioned above.

The contrast of the SDSS spectrum of SDSS 0944 with that shown by Jiang et al. (2000) reveals that the Balmer lines are less optically thick (the Balmer decrement is closer to the recombination values) and the accretion disk has a lower density (the M star is dominating redward of 5000 Å) at the time of the APO observations. However, as noted above, this system has a large amplitude orbital modulation, so the appearance of the secondary star is more noticeable at some phases than others.

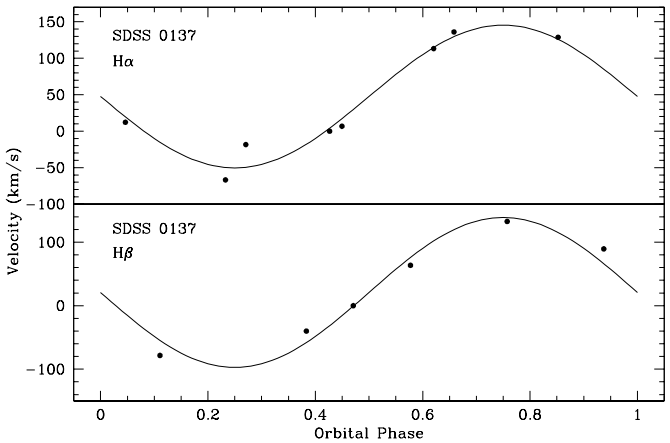

FIG. 25.—Same as Fig. 23, but for SDSS 0137

TABLE 5
ROSAT DETECTIONS

SDSS	*ROSAT* (counts s^{-1})[a]	Exp. (s)	RXS
0853.....	0.41 ± 0.04	394	J085343.5+574846 (=BZ UMa)
0944.....	0.09 ± 0.02	243	J094432.1+035738
1137.....	0.03 ± 0.01	243	J113723.5+014847 (=RZ Leo)
1138.....	0.66 ± 0.06	410	J113826.8+032210 (=T Leo)
1146.....	0.023 ± 0.007	689	J114631.3+675932
1243.....	0.125 ± 0.035	141	J124326.5+025603
1258.....	0.03 ± 0.01	477	J125837.1+663608
1446.....	0.04 ± 0.01	345	J144700.9+025344
1700.....	0.07 ± 0.01	744	J170053.7+400354
2050.....	0.04 ± 0.01	329	J205018.4−053631
2258.....	0.17 ± 0.04	145	J225834.4−094945

[a] For a 2 keV bremsstrahlung spectrum, 1 count s^{-1} corresponds to a 0.1–2.4 keV flux of about 7×10^{-12} ergs cm^{-2} s^{-1}.

3.6. *ROSAT Correlations*

The cross-identification of the new CVs with the X-ray *ROSAT* All Sky Survey (RASS; Voges et al. 1999, 2000) reveals that 11 are X-ray sources or have X-ray detections close to their positions. Of these, the three known dwarf novae (BZ UMa, RZ Leo, and T Leo) all have X-ray emission, as well as the *ROSAT*-identified CV RX J094432.1+035738 and our newly confirmed polar SDSS 1700. Table 5 lists the objects and their RASS count rates. Since SDSS 1446 has no polarization, yet is an X-ray source with strong He II emission, it may be an IP.

4. CONCLUSIONS

The 42 objects here combined with the 22 in Paper I give a total of 64 CVs from 325 plates or an areal density of about 0.03 deg^{-2}. This represents a lower limit to the density of CVs, since not all possible CV candidates (by color) are targeted for spectra. In the future, we hope to use the plate overlap sections to accomplish identifications by a combination of variability and color that will provide us with a measure of completeness. However, even with the selection obtained, SDSS is picking up a wide variety of new CV systems, including those with high mass transfer rates (SW Sex stars), as well as the faintest systems with the lowest mass transfer rates and coolest white dwarfs yet found among CVs (Szkody et al. 2003). Of the 35 new discoveries reported here, about a third show characteristics that indicate they are likely candidates for having a magnetic white dwarf. Another third indicate very low mass transfer rates (from visibility of the underlying stars or from very large emission line fluxes and low continuum). From the follow-up data available for 26 of the systems, three have shown eclipses. The majority of the orbital periods determined so far are under the period gap, indicating that SDSS is predominantly finding the lowest mass transfer, shortest orbital period systems that brighter surveys have missed, for example, the PG survey (Green et al. 1982) and the Hamburg survey (Hagen et al. 1995). With an aperture of 3.5 m, we are currently limited in follow-up work to systems brighter than 19th magnitude. It will take larger telescopes to determine the nature of the faintest CVs being found. However, by the end of the SDSS, we

should have a clearer picture of the range of parameters and the distribution of types of CVs in the galaxy, including both high and low accretion rate systems.

We gratefully acknowledge Michael Strauss and Patrick Hall for pointing out some of the CV candidates and Don Schneider for useful comments on the manuscript. Funding for the creation and distribution of the SDSS Archive has been provided by the Alfred P. Sloan Foundation, the Participating Institutions, the National Aeronautics and Space Administration, the National Science Foundation, the US Department of Energy, the Japanese Monbukagakusho, and the Max Planck Society. The SDSS Web site is http://www.sdss.org/. Studies of magnetic stars and stellar systems at Steward Observatory is supported by the NSF through AST 97-30792. The SDSS is managed by the Astrophysical Research Consortium (ARC) for the Participating Institutions. The Participating Institutions are the University of Chicago, Fermilab, the Institute for Advanced Study, the Japan Participation Group, Johns Hopkins University, Los Alamos National Laboratory, the Max-Planck-Institut für Astronomie (MPIA), the Max-Planck-Institut für Astrophysik (MPA), New Mexico State University, University of Pittsburgh, Princeton University, the US Naval Observatory, and the University of Washington. P. S. and S. L. H. also acknowledge support from NSF grant AST 02-05875 and an RRF grant from the University of Washington.

REFERENCES

Beers, T. C., Rossi, S., Ulrich, D., & Wilhelm, R. 1996, AJ, 112, 1188
Berg, C., Wegner, G., Foltz, C. B., Chaffee, F. H., & Hewett, P. C. 1992, ApJS, 78, 409
Berger, J., & Fringant, A. M. 1984, A&AS, 58, 565 (BF84)
Bond, H. E., White, R. L., Becker, R. H., & O'Brien, M. S. 2002, PASP, 114, 1359
Downes, R. A., Webbink, R. F., M. M., Ritter, H., Kolb, U., & Duerbeck, H. W. 2001, PASP, 113, 764 (D01)
Fukugita, M., Ichikawa, T., Gunn, J. E., Doi, M., Shimasaku, K., & Schneider, D. P. 1996, AJ, 111, 1748
Green, R. F., Ferguson, D. H., Liebert, J., & Schmidt, M. 1982, PASP, 94, 560
Gunn, J. E., et al. 1998, AJ, 116, 3040
Hagen, H. J., Groote, D., Engels, D., & Reimers, D. 1995, A&AS, 111, 195
Hogg, D. W., Finkbeiner, D. P., Schlegel, D. J., & Gunn, J. E. 2001, AJ, 122, 2129
Howell, S. B., Rappaport, S., & Politano, M. 1997, MNRAS, 287, 929
Howell, S. B., & Szkody, P. 1988, PASP, 100, 224
Jiang, X. J., Engels, D., Wei, J. Y., Tesch, F., & Hu, J. Y. 2000, A&A, 362, 263 (J00)
Lupton, R. H., Gunn, J. E., Ivezić, Ž., Knapp, G. R., Kent, S. M., & Yasuda, N. 2001, in ASP Conf. Ser. 238, Astronomical Data Analysis Software and Systems X, ed. F. R. Harnden, Jr., F. A. Primini, & H. E. Payne (San Francisco: ASP), 269
Lupton, R. H., Gunn, J. E., & Szalay, A. 1999, AJ, 118, 1406
Mennickent, R. E., & Tappert, C. 2001, A&A, 372, 563 (MT01)
Patterson, J. 1984, ApJS, 54, 443
Pier, J. R., Munn, J. A., Hindsley, R. B., Hennessy, G. S., Kent, S. M., Lupton, R. H., & Ivezić, Ž. 2003, AJ, 125, 1559
Rodríguez-Gil, P., Casares, J., Martínez-Pais, I. G., Hakala, P., & Steeghs, D. 2001, ApJ, 548, L49
Shafter, A. W. 1983, ApJ, 267, 222
Smith, J. A., et al. 2002, AJ, 123, 2121
Stoughton, C., et al. 2002, AJ, 123, 485
Szkody, P., et al. 2002, AJ, 123, 430 (Paper I)
———. 2003, ApJ, 583, 902
Voges, W., et al. 1999, A&A, 349, 389
———. 2000, IAU Circ., No. 7432
Warner, B. 1995, in Cataclysmic Variable Stars (Cambridge: Cambridge Univ. Press)
Wegner, G., & Boley, F. I. 1993, AJ, 105, 660
Wolfe, M., Szkody, P., Fraser, O., Homer, L., Skinner, S., & Silvestri, N. M. 2003, PASP, in press
York, D. G., et al. 2000, AJ, 120, 1579